Statistical analysis of the observations of the MEX/ASPERA-3 NPI in the shadow

A. Milillo [a,*], A. Mura [a], S. Orsini [a], S. Massetti [a], P.C. son Brandt [b], T. Sotirelis [b], R. D'Amicis [a], S. Barabash [c], R.A. Frahm [d], E. Kallio [e], A. Galli [f], P. Wurz [f], M. Holmstrom [c], E.C. Roelof [b], J.D. Winningham [d], P. Cerulli-Irelli [a], S. Livi [d], R. Lundin [c], M. Maggi [a], A. Morbidini [a]

[a] INAF/Instituto di Fisica dello Spazio Interplanetario, via del Fosso del Cavaliere 100 Rome, Italy
[b] Applied Physics Laboratory, Johns Hopkins University, Laurel, USA
[c] Swedish Institute of Space Physics, Kiruna, Sweden
[d] SouthWest Research Institute, San Antonio, USA
[e] Finnish Meteorological Institute, Helsinki, Finland
[f] University of Bern, Physikalisches Institut, Bern, Switzerland

ARTICLE INFO

ABSTRACT

The analyser of space plasma and energetic atoms (ASPERA-3) neutral particle imager (NPI) on board Mars Express (MEX) is devoted to energetic neutral atom (ENA) detection within the Martian environment. These ENAs originate from the interaction between the energetic ions flowing inside the Martian environment and the exospheric neutral gas, thus providing crucial information about the dynamics of this interaction. NPI records the instantaneous angular distribution of the energy-integrated ENA signal. In order to identify recurrent ENA signals in the Martian environment, we have performed a statistical analysis of the NPI data. Count rates have been averaged using different methods in order to be able to discriminate signals coming from the planet, from a selected direction, or from specific planetographic regions at the planetary surface. Possible recurrent ENA signals (about $5 \times 10^6 \, (\text{cm}^2 \, \text{sr} \, \text{s})^{-1}$) are found coming from the terminator direction and above the atmosphere toward nightside when the spacecraft was inside the planetary shadow, mainly close to the shadow edge. Some significant signal was found from the anti-Mars directions in 2005. No statistically significant signal related to pick-up ions from the atmosphere or related to magnetic anomalies above the sensor intrinsic error (estimated as $3 \times 10^6 \, (\text{cm}^2 \, \text{sr} \, \text{s})^{-1}$) was observed. Our analysis shows that particular attention should be given to the use of NPI data when performing statistical studies; in fact, the sensor has some intrinsic limitations due to inadequate UV suppression, difficulties in sector inter-calibrations, and variations in the sector response versus time.

© 2008 Elsevier Ltd. All rights reserved.

1. Introduction

The plasma and neutral particle package, analyser of space plasma and energetic atoms (ASPERA-3) (Barabash et al., 2004), has been operating on board ESA Mars Express (MEX) spacecraft since orbit insertion in December 2003. The ASPERA-3 instrument that includes four sensors: an electron spectrometer (ELS), an ion analyser (IMA), and two different energetic neutral atom (ENA) sensors: the neutral particle imager (NPI, an ENA imager with high angular resolution, but with no mass and energy resolution) and the neutral particle detector (NPD, a neutral mass analyser that can resolve both particle velocities and masses, with lower

angular resolution). NPI is devoted to ENA imaging of the signal generated in the Martian environment by the interaction between the solar wind (SW) and the upper atmosphere.

Since the SW interacts with Mars mainly through the ambient atmospheric/exospheric gas (Kallio et al., 1997, 2006), charge-exchange is expected to be very effective. Several numerical simulations have been performed to study such interaction, including different ion/neutral sources: supersonic and shocked SW (Holmström et al., 2002), and accelerated planetary ions (Barabash et al., 2002; Lichtenegger et al., 2002). Charge-exchange ENAs may also emerge from the SW interaction with the atmosphere of Phobos (Mura et al., 2002). Other processes, like atmospheric atoms sputtered by picked-up O^+ ions (Johnson and Luhmann, 1998) and SW protons backscattered from the Martian exosphere (Kallio and Barabash, 2001; Holmström et al., 2002), can be responsible for additional neutral emission. Hence, ENA

* Corresponding author.
E-mail address: anna.milillo@ifsi-roma.inaf.it (A. Milillo).

imaging is a potentially useful tool to understand the geometry, the physics, and the dynamics of the plasma and the escape mechanisms around Mars.

ENA signals have been detected and fruitfully analysed in dedicated studies of specific events by the ASPERA-3/NPD sensor (e.g., Futaana et al., 2006; Galli et al., 2006) and by the NPI sensor on the nightside (Brinkfeldt et al., 2006; Gunell et al., 2006). Mura et al. (2007) and Galli et al. (2008) successfully performed a statistical analysis of the NPD ENA data from the dayside and nightside, respectively.

In order to identify recurrent ENA signals in the Martian environment, we have performed a statistical analysis of the available NPI data covering two time periods: from January 25th 2004 up to September 15th 2005 and from September 24th up to December 14th. We have averaged the data using several methods in order to be able to discriminate between those signals which come from the planet, and those which come from selected directions depending on relative Sun positions or those which come from specific locations close to the surface, possibly linked to planetary features like magnetic anomalies.

In this paper, we will present a brief description of the NPI characteristics and the MEX position during the eclipse seasons in Section 2 followed by a description of the possible nightside ENA sources that the present analysis intends to discuss in Section 3. In Section 4, the statistical analysis procedure used to analyse the NPI data is described. From this process, maps of the average signal as emitted from the planet are created and are described in Section 5. In Section 6, the maps for each spacecraft position during eclipse seasons, obtained by averaging the signal for specific look directions, are discussed. The maps of the emitted signal coming from specific planetary regions have been obtained by considering the planetographic coordinates and comparing them to magnetic anomaly maps (Section 7). The summary and conclusions of this work are given in Section 8.

2. Neutral particle imager

NPI (Fig. 1) measures the integral ENA flux (in the energy range 0.1–60 keV) without mass and energy resolution, but with good angular resolution, $4.5° \times 11.25°$ (Barabash et al., 2004). The incoming ENAs are reflected by a coated target block before being detected by a 32 sector anode, covering a total $360° \times 5°$ field-of-view (FOV). In its MEX configuration, NPI sectors 15 and 16 are physically blocked by the spacecraft. The time resolution of the data collected in a telemetry packet is 1 s. The geometrical factor of each sector is $G = 2.7 \times 10^{-3}$ cm^2 sr, while the efficiency of the instrument is energy dependent (e.g., for 1 keV neutrals $\varepsilon = 4 \times 10^{-4}$) (Holmstrom et al., 2006; Brinkfeldt, 2005). Hence, a count rate of 1 s^{-1} would correspond to a 1 keV flux of $f = 1/G, \varepsilon = 9 \times 10^5$ (cm^2 sr s)$^{-1}$.
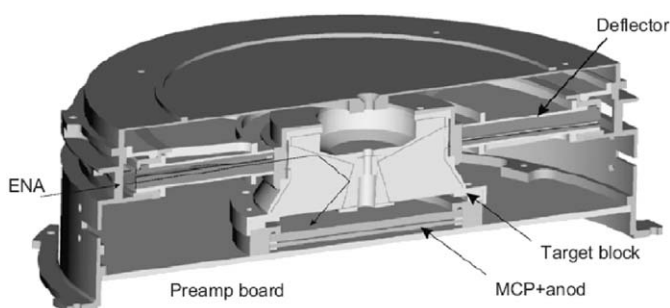
Fig. 1. NPI geometry.

The NPI detector is known to be strongly affected by UV contamination; hence, a careful data analysis is needed. Furthermore, Holmstrom et al. (2006) have shown that different sectors have different responses to ENAs, with varying sensitivity, β, and background noise levels, α. Moreover, the α values show time variations. In order to avoid the UV contamination, we have selected only those data collected during periods of spacecraft eclipse. This is known as deep-shadow condition (sdw). Solar eclipse positions were selected since outside of this region, sectors in the anti-sun direction are found to be affected by electronic cross-talk caused by Solar UV (Holmstrom et al., 2006). Furthermore, atmospheric UV emission is observed outside of eclipse and it must be avoided as well.

Figs. 2a and b show the spacecraft position during the eclipse seasons of 2004 and 2005, respectively. The spacecraft is mostly in the Southern hemisphere during 2004; whereas, it is mainly in the Northern hemisphere during 2005. Note that NPI was not always operative during the eclipse periods.

3. ENA sources in the shadow of Mars

A likely source of ENAs results from charge-exchange of the SW with the atmosphere. However, since we impose the sdw, we are investigating ENAs produced by deflected SW which has a velocity component perpendicular to the shadow cylinder of the planet. In fact, theoretical models (e.g., Kallio et al., 2006) foresee that the shocked SW inside the Mars magnetosheath produces ENAs directed tailward that, thanks to non-zero temperature, have a component toward the planet shadow. A proof of this ENA signal was recently obtained by Galli et al. (2008) from the 23 April to 26 May 2004 statistical analysis of NPD data, when the spacecraft was in the nightside of Mars and inside the induced magnetosphere boundary. The ENA signal between 0.2 and 10 keV has maximum intensity $(2.4 \times 10^5$ cm^{-2} s^{-1} sr^{-1}) for look directions, which are closest to the planet terminator (i.e., the limb close to the Sun direction). The observed ENA signal comes from a broader region (look directions extending more than 60° from the limb) than that expected by theoretical models. Hence, ENAs seem to be generated mainly close to the planetary terminator, but also in a broad region above the planet. Galli et al. (2008) suggested that the contribution of planetary ions should be responsible for such a discrepancy. In this case, pick-up ions can also be a source for ENAs. The generated ENAs should again come from close to the terminator toward the nightside, but in this case they should be preferentially lost in the direction of the electric field (Fedorov et al., 2006). An IMF clock angle asymmetry in ENA signal would be a proof that such a generation mechanisms is active.

Backscattered ENAs in the dayside have been reported by Futaana et al. (2006). The same process could, in principle, occur when ions precipitate toward the nighside atmosphere from the tail. Galli et al. (2008) estimated an upper limit of about 10^4 cm^{-2} s^{-1} sr^{-1} for this ENA signal.

Finally, another possible ENA generation region could be related to magnetic anomalies (Purucker et al., 2000). Magnetic anomalies trap electrons (Mitchell et al., 2007) and can, in principle, trap ions as well. In fact, if this is the case, trapped ions can charge-exchange with atmospheric neutrals thus generating radiating ENAs. This process can also occur on the planet's nightside toward the dusk terminator. The ENA signal should decrease on the nightside of Mars toward dawn as the electrons and ions trapped in the minimagnetospheres recombine during the planet rotation.

4. Data analysis

In our analysis we have used the count corrections computed for the years 2004 and 2005, as estimated in Holmstrom et al. (2006).
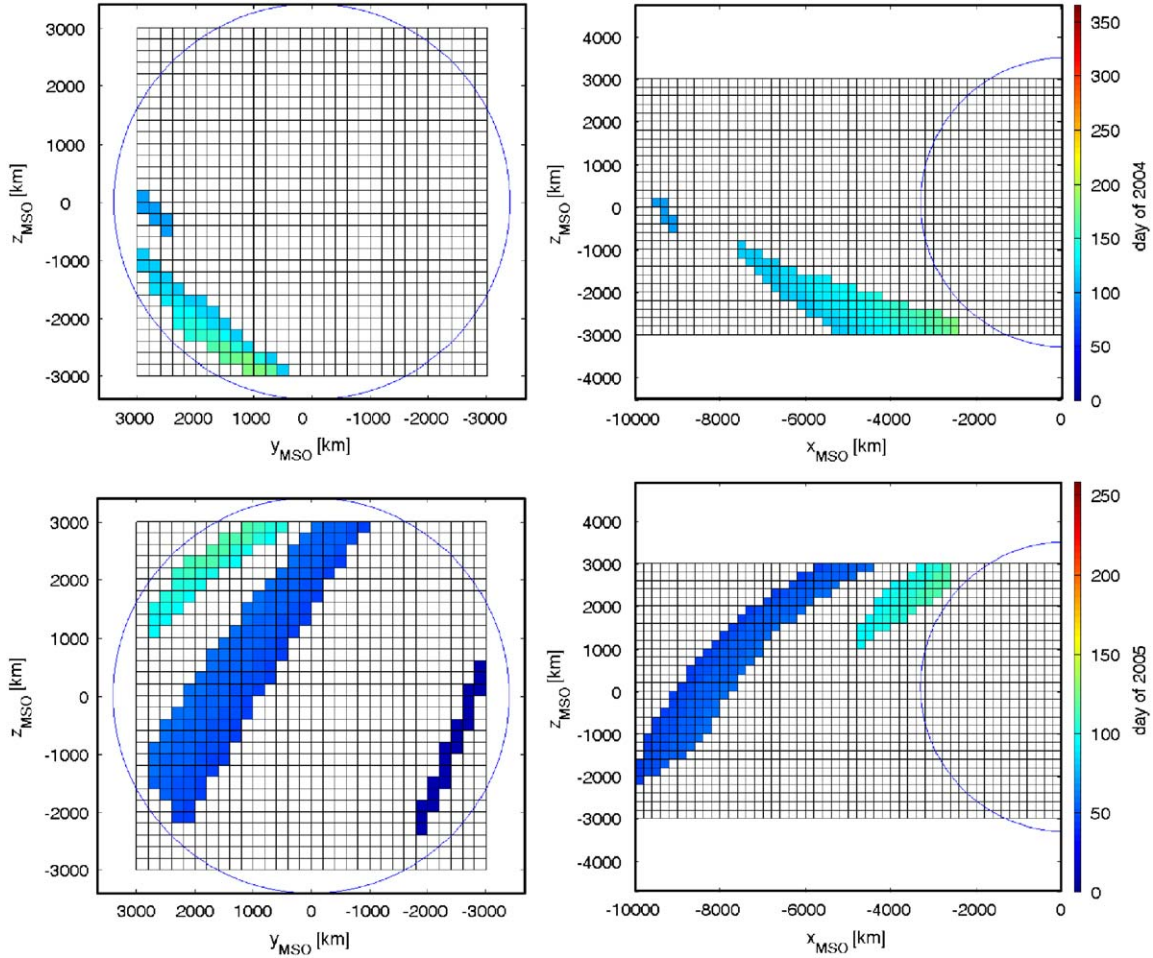
Fig. 2. Position during eclipse seasons in 2004 ((a) yz_{MSO} plane; (b) xz_{MSO} plane) and in 2005 ((c) yz_{MSO} plane; (d) xz_{MSO} plane). The colour-code is only a way of indicating the corresponding time for each projection.

By considering the sensitivity β_i and the noise level α_i as mentioned in Section 2, the data have been noise reduced for each sector i using the formula given by Holmstrom et al. (2006)

$$v_i = \frac{(u_i - \alpha_i)}{\beta_i} \tag{1}$$

where u_i and v_i are the raw and corrected counts, respectively. These corrected data are then mapped into various coordinate systems. One of these coordinate systems is in Mars centric coordinates, the data collected in spacecraft reference frame were converted into the MSO coordinate system (Mars–Sun orbital: where x_{MSO}-axis points from Mars toward the Sun, y_{MSO}-axis points opposite to the orbital motion of Mars, and z_{MSO}-axis completes the right-hand coordinate system).

Data were collected when the spacecraft met the "deep-shadow" condition (sdw)

$$x_{MSO} < 0 \text{ km}$$
$$\sqrt{y_{MSO}^2 + z_{MSO}^2} < R_{sdw} \tag{2}$$

where $R_{sdw} = 3000$ km (the Mars radius is $R_M \sim 3400$ km). The sdw was imposed in order to reduce contamination in the data by UV light scattered at the terminator of Mars by the upper atmosphere.

The different statistical analyses presented in the following intend to evidence the different possible ENA sources described before.

Numerical simulations show that the atmosphere forms an obstacle between 100 and 200 km altitude which prevents the SW from reaching the planet surface (Kallio, 1996). Since most of ENAs are generated close to the planet where the neutral gas density is higher, we have projected the signal from each of the sectors central look direction onto a sphere of radius $R_O = 3500$ km centered on Mars, with 10° latitude and 15° longitude spacing (i.e. 1 h of local time (LT)) gridding. Note that the intrinsic error in the angle definition is the sector angular coverage (11.25°). This error can produce maps in which blurring of data is much more pronounced when spacecraft is at more distant positions. For each grid cell (mn) we have computed the averaged counts (C_{mn}), the standard deviation (E_{mn}) and the signal to error ratio (σ_{mn}). Since the data generally have high E_{mn}, it is important, in order to be confident with the statistical analysis, to have a significant data sample. Hence, only averages with the number of samples $N_{mn} > 300$ have been considered statistically significant and the sectors showing the noisiest data (largest standard deviation) are excluded from further study (see Section 5).

We have analysed the signal arising from specific look directions by defining the angles from the limb direction, where we have assumed a circular symmetry about the Mars–Sun line. A sketch of the geometry of the NPI look directions is shown in Fig. 3, where λ is the angle between the nadir and the limb directions, and φ is the angle between the look direction of each sector and the limb direction. Note that directions symmetrically oriented with respect to the nadir are averaged together. For each

MEX position, φ ranges from $-\lambda$ (nadir) to $180° - \lambda$ (zenith) ($\varphi < 0°$ means directions toward the planet). For maps created using MSO coordinates, the average count of the sectors in the selected look direction range is mapped according to MEX position projected on the yz_{MSO} plane. When the Martian planetographic maps have been produced, a $10°$ latitude $-10°$ longitude spacing gridding has been used on the R_O sphere.
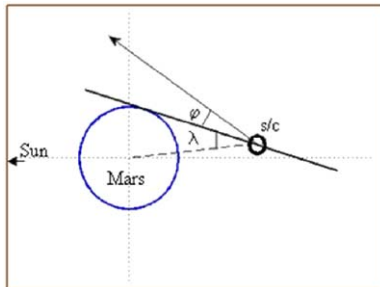
Fig. 3. Geometry of the sector look directions, φ, and the nadir direction, λ, with respect to the limb direction.

5. Maps of NPI signal from the planet

As a first step, we have considered all NPI data, not only those in the deep shadow. Hence, we have computed a LT versus latitude map (Milillo et al., 2007) by assuming an ENA emission source at about 100 km altitude and averaging the corrected counts of those sectors pointing to specific locations. In this case (not shown here), most of the signal comes from the dayside reaching more than 100 counts/(s sector). Although an ENA albedo is expected and has been detected by NPD (Futaana et al., 2006, Mura et al., 2007) most of the signal at NPI is caused by UV albedo from the Martian atmosphere (UV albedo from the planet surface is negligible due to atmospheric absorption).

For this reason, UV contamination was tentatively excluded by selecting the MEX deep-shadow positions (Eq. (2)) (we cannot exclude the galactic and stellar UV sources). We have tested the sector inter-calibration by averaging the signal of each sector for the period from January 25th 2004 up to September 15th 2005. In this case, if the sectors point on average at similar positions in space, the fluctuation of counts of different sectors should be almost 0. In Fig. 4a and b the averaged counts of the NPI sectors (dashed line) and the corrected counts by Eq. (1) (solid line) are
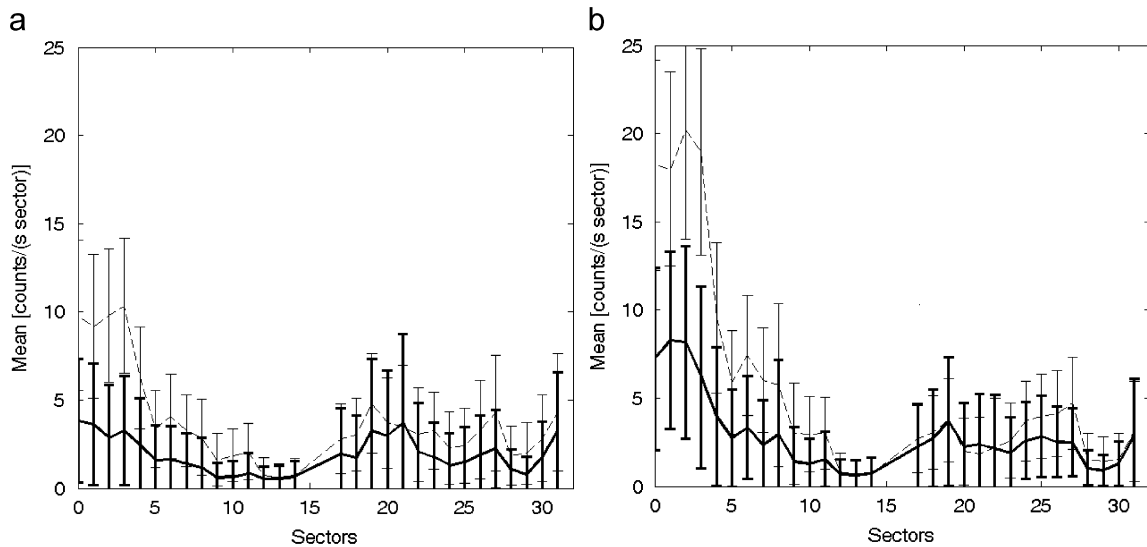
Fig. 4. Averaged sector response: not calibrated (dashed) and calibrated (solid) during eclipse seasons. (a) 2004 and (b) 2005.
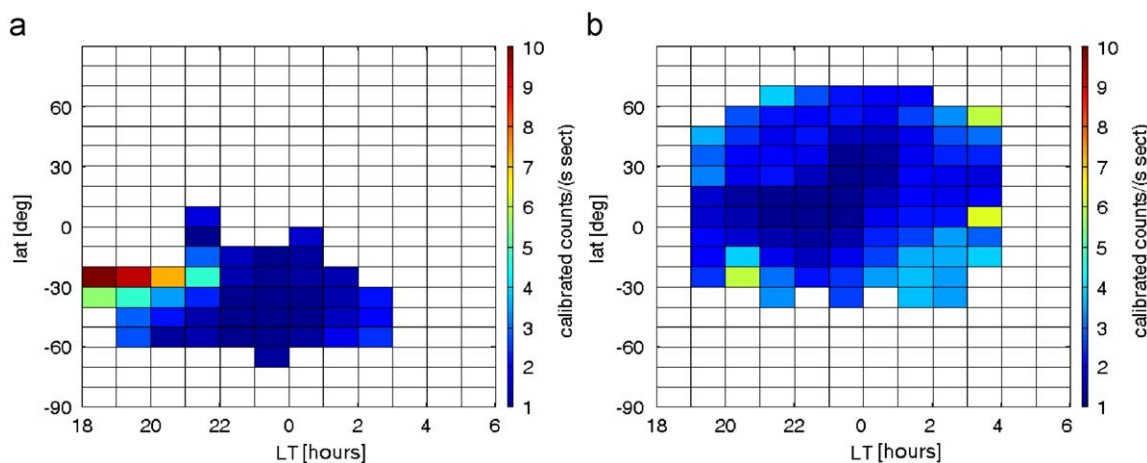
Fig. 5. NPI signal (counts/(s sector)) mapped at an altitude of 100 km from Mars surface in MSO coordinates, for 2004 (a) and 2005 (b) when MEX position is in the deep shadow. Sectors 0–3 are excluded from the analysis.

plotted for 2004 and 2005, respectively. The plotted error bars are the standard deviations. We can see that generally the averaged response is higher for sectors 0–3. The response is more uniform after the calibration, but some fluctuations are still present, especially for the 2005 data where the error bars indicate a significant systematic error in the first four sectors. From these plots we can state that, if we exclude sectors 0–3, the intrinsic error (i.e. the maximum fluctuation of sectors 4–31) of the statistical analysis is about 3.5 counts/(sector s).

By excluding sectors 0–3 from the analysis of positions within the deep shadow, the resulting maps for the 2 years are shown separately in Fig. 5. We can see that the signal resulting from the selected data is strong close to the terminator. The 2004 map Fig. 5a indicates that a stronger signal is coming from a specific West look direction, while the 2005 map Fig. 5b indicates a more uniform intensification (above the intrinsic error) close to the terminator. This difference can be explained by the different look direction geometries of NPI during the 2 years (some more speculations about this point will be discussed in the next section). This feature could be interpreted as ENAs coming from the dayside generated by the SW and heated by collision with the dense atmosphere (Kallio et al., 2006), but alternatively it could be the scattered UV from the atmosphere (Brinkfeldt et al., 2006).
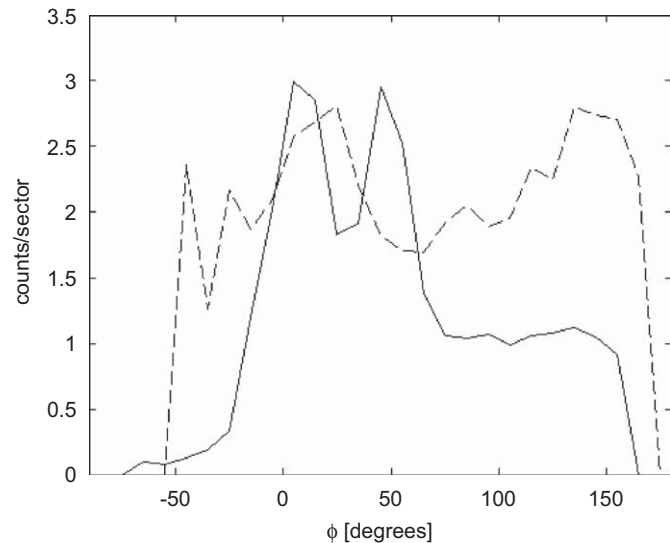
Fig. 6. Averaged signal versus angle, φ, from the limb for the 2 years: 2004 (solid line) and 2005 (dashed line). Sectors 0–3 are excluded.
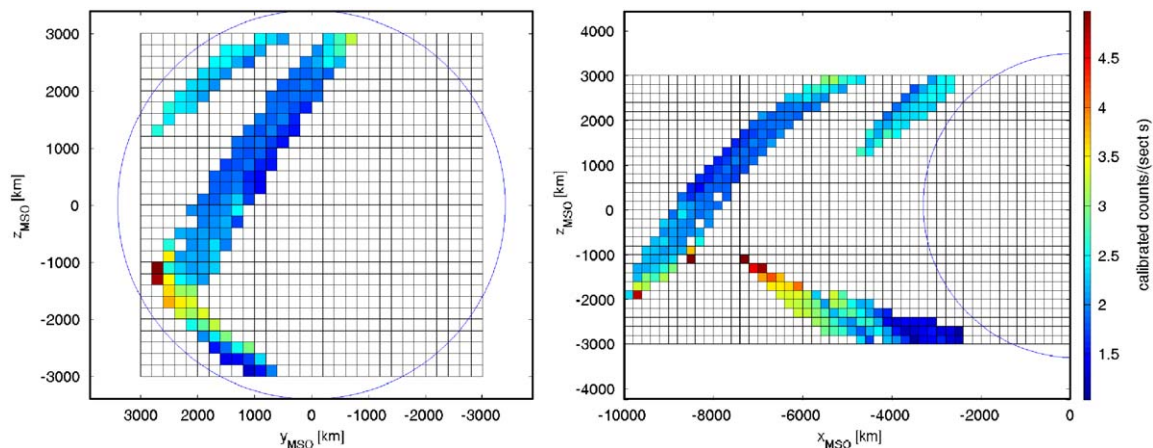
Using the estimated calibrated data factor of Section 2, the maximum ENA flux in 2004 case is about $8 \times 10^6 \, (cm^2 \, sr \, s)^{-1}$ and in 2005 is about $5 \times 10^6 \, (cm^2 \, sr \, s)^{-1}$. This signal is found to be strongly variable in time, since we found that the σ values (see Milillo et al., 2007) are generally high close to the terminator. This means that if this signal is due to ENA, the flux is not strongly dependent by SW conditions.

6. NPI signal from selected look directions

We have investigated the preferential directionality of the signal by plotting in Fig. 6 the averaged signal versus angle from limb (φ) for the 2 years: 2004 (solid line) and 2005 (dashed line). A signal at $-10° < \varphi < 60°$ is evident in 2004 and also visible in 2005 with similar intensity. The low signal intensity (3 counts/(s sector)) and the low σ (generally close to the unity) cannot allow a strong confidence in the results and can explain the visible differences in shapes of the two curves. This signal could be due to scattered UV light and/or ENAs coming from the limb nearby. Since in the selected MEX positions the limb is mostly close to the terminator, this result is in agreement with the analysis described in Section 4. Unexpectedly, in 2005 a similar high-intensity signal is seen well away from Mars ($90° < \varphi < 150°$) and is also distinguishable in Fig. 6 above the 2004 signal level.

Fig. 7 shows the 2004 and 2005 maps obtained according to MEX position, by considering only the sectors where $-10° < \varphi < 60°$, i.e., viewing directions near and above the limb. The averaged signal is generally higher (maximum 5 counts/(s sector) when MEX is close to the edge of the shadow and close to apo-center for both years. This result seems to be consistent with the analysis of the NPD ENA data by Galli et al. (2008). In fact, they concluded that an ENA signal is observed from the nightside close to the limb, in particular when the look directions were toward the Sun. Furthermore, they concluded that this signal extends further outward from the planet limb than is predicted based on simple SW–atmosphere interaction models. The angular resolution of NPD sensor is coarse ($30°$); nevertheless, they estimated an opening angle from the Sun direction of about $60°$. If we consider in our analysis an average MEX position in the nightside along the Mars–Sun line (x_{MSO}-axis), their result is in good agreement with our result. The near-limb ENA flux intensity estimated from the calibrated data described in Section 2 is at maximum $4.5 \times 10^6 \, (cm^2 \, sr \, s)^{-1}$. This estimated flux is one order of magnitude higher than the ENA flux derived by the Galli et al. (2008) study, i.e. $2.4 \times 10^5 \, (cm^2 \, sr \, s)^{-1}$. As mentioned in Section 3,

Fig. 7. Averaged signal coming from $-10° < \varphi < 60°$ mapped according to MEX position projected in the yz_{MSO} plane (*left*) and in the xz_{MSO} plane (*right*) for the 2 years together. Sectors 0–3 are excluded.

a possible source of this signal could be planetary pick-up ions interacting with Martian upper atmosphere.

In order to investigate the possible relation with pick-up ions, NPI observations between the day of the year 269 and 349 of 2005

Fig. 8. Averaged signal from sectors directed within 15° of sunward, organized in 15°-bins by spacecraft location in the yz_{MSO} plane, for three different 90° IMF clock angle intervals: northward (upper panel), duskward (middle panel) southward (lower panel). Sectors 0–3 are excluded.

were binned by IMF clock angle. The IMF clock angle was determined from Mars Global Surveyor (MGS) magnetometer observations in the dayside sheath (Brain et al., 2006), and are considered accurate to only $\pm 90°$ (since the correspondence between the clock angle in the sheath field and in the IMF is only approximate). The eclipse condition for this analysis was that MEX be at least $0.15 R_M$ and within the umbra.

Counts from sectors directed within 15° of sunward were binned by spacecraft location in the y–z MSO plane. For data where the spacecraft met the sdw, plots of the average corrected counts collected in $0.1 R_M$ by 15° bins are shown in Fig. 8, for three different 90° IMF clock angle intervals (the interval centered on dawnward are not shown since they had insufficient coverage). At least 100 observations per bin were required.

The signal intensification close to the terminator direction reaches in this case 16 counts/s (equivalent to an ENA flux of $10^7 (cm^2 sr s)^{-1}$). No systematic IMF clock angle dependence is evident, above the intrinsic error. This suggests that, if the signal is caused by ENAs and not by UV, the ENAs detected here by NPI are not caused by pick-up atmospheric ions, but are so-called SW ENAs produced by charge-exchange between SW protons and the Martian exosphere. Anyway, the observed broad distribution from the limb remains unexplained. Moreover, noise related to UV photons can hardly produce that broad of the signal. Further investigation is needed to solve this issue.

In order to investigate the signal observed when viewing away from Mars suggested by Fig. 6, we have created the maps of Fig. 9. This figure shows the maps obtained by considering only the sectors pointing at $90° < \varphi < 150°$. Fig. 9 shows that the signal is faint in 2004, while in 2005 it reaches 4 counts/(s sector) when MEX is at latitudes between 10° and 40° in the dusk sectors. Although the maps have been created by excluding the bad sectors (0–3), we have noticed that this signal is much more pronounced when all the sectors are included in the analysis (reaching 9 counts/(s sector)). Hence, since the signal intensity is of the order of the intrinsic error (see Section 4), a bad sector inter-calibration could be the cause of this enhanced signal. Effectively, by comparing these maps with the time evolving maps of MEX position (Fig. 2) we can see a relation between counts and time (the North-West signal is also the last considered period of shadow of this analysis). This suggests that a possible variation in the background noise levels, α, of some sectors during April–May 2005 could be the cause of this signal. This signal could also be due to ENAs produced by ions directed from the tail toward the planet, but this does not seem reasonable since an upper limit for this signal was estimated to be $10^4 (cm^2 sr s)^{-1}$ (Galli et al., 2008).
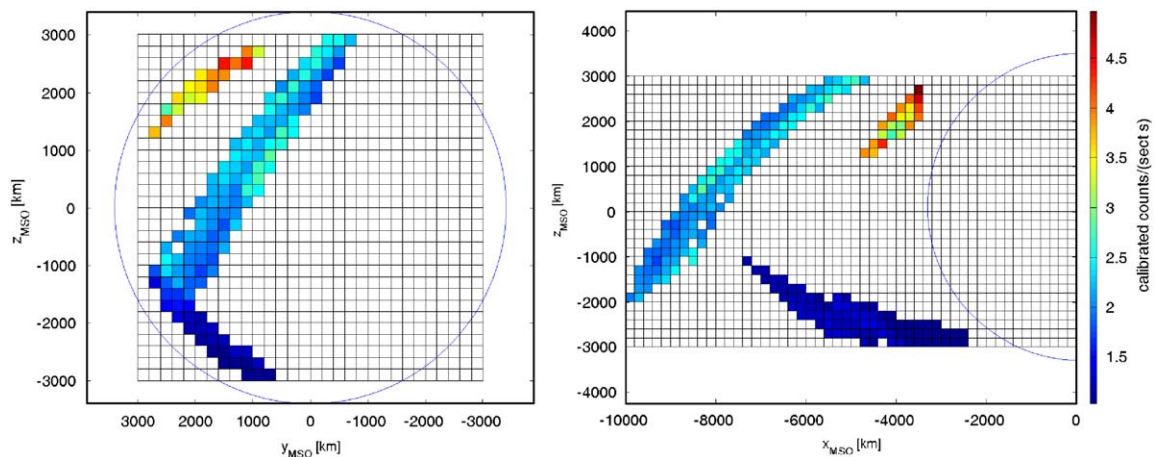
Fig. 9. Averaged signal coming from $90° < \varphi < 150°$, mapped according to MEX position, projected in the yz_{MSO} plane (*left*) and in the xz_{MSO} plane (*right*) for the 2 years together. Sectors 0–3 are excluded.

Alternatively, another explanation could be that during 2005 the UV disturbance due to the Milky Way is more prominent in the FOV of the instrument (Holmstrom et al., 2006).

7. Planetographic maps

A signal arising from specific planetographic locations (e.g., related to the magnetic anomalies discovered on the Mars surface) can only be identified when all the other sources of the signal have been removed and when the data are mapped in planetographic coordinates.

In Fig. 10 the planetographic maps of signals from the planet for 2004 (left) and 2005 (right) are shown. In 2004, higher counts are observed at latitudes within 30° of the equator and lower counts are observed outside of this region. This is in contrast to the counts from 2005 which show no striking latitudinal dependence.

These maps are affected by the limb signal shown previously in Section 4. In order to exclude the limb signal, we have created another map by considering only the sectors pointing toward the planet at an angle from the limb of $\varphi < -10°$ (Fig. 11). These selected NPI count rates are unfortunately less than the intrinsic error on an average (generally <3 counts/(s sector)). The count rates shown could be due to the interaction between plasma temporarily confined in the magnetic loops and the local atmospheric atoms producing charge-exchange ENAs. If this is the case, we would expect that features of Fig. 11 should match the map of the magnetic anomalies as derived by other instruments on board Mars Global Surveyor. The map of magnetic field polarity derived by the magnetometer (Purucker et al., 2000) and the map of magnetic field intensity derived by the magnetometer/electron reflectometry experiment (Mitchell et al., 2007) refer to an altitude of about 170 km (which is about the reference altitude of our maps).

Unfortunately, we cannot see any clear correlation above the intrinsic error between the NPI signal and the magnetic anomalies, neither in polarity, nor in magnetic field intensity.

8. Conclusions

This study investigates whether it is possible to discover recurrent ENA signals by a statistical analysis of the NPI data. Unfortunately, the NPI sensor is likely to have some intrinsic limitations due to: (i) insufficient UV suppression, (ii) difficulties in sector inter-calibrations, and (iii) the variation of sector response versus time. In order to minimize the UV contamination we have selected events when MEX was in the shadow of Mars. We have calibrated the sectors and, in order to increase the reliability of the results, we have also excluded sectors 0–3 that show a residual anomalous response.

We have investigated the existence of ENAs within the optical shadow. Possible results are summarized in the following:

- A signal coming from look directions close to the Mars terminator toward the nightside has been identified. It can be due to ENAs coming from the dayside generated by the SW and heated by collision with the dense atmosphere (Kallio et al., 2006) and/or scattered UV by the atmosphere.
- Strictly related to the signal close to the terminator is the signal from a few degrees of the limb, when the spacecraft is far from the planet and close to the edge of the shadow. A similar feature, identified as SW ENAs produced by charge-exchange between SW protons and the Martian exosphere, has been shown by Brinkfeldt et al. (2006) in a case study by using NPI data. Galli et al. (2008) by using NPD data explained the broad ENA signal from the limb as generated by planetary ions. While the shape of the signal obtained by this analysis (extension of about 60° away from the planet) seems in good agreement with their study, a tentatively estimate of the ENA flux (about $4 \times 10^6 (cm^2 \, sr \, s)^{-1}$) is more than one order of magnitude higher than the flux estimated by Galli et al. (2008). Anyway,
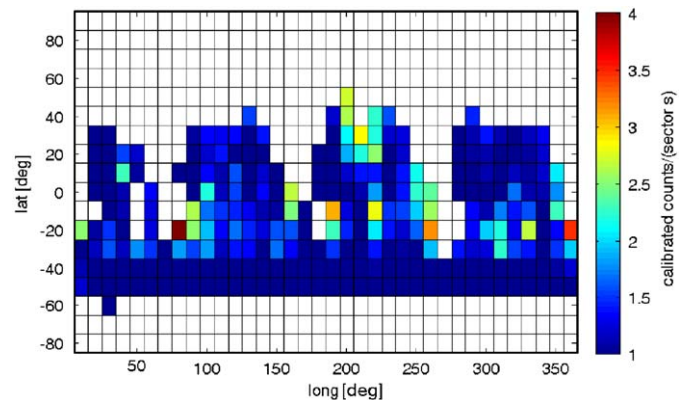
Fig. 11. NPI signal (counts/(s sector)) mapped on Mars surface in planetographic coordinates, for the whole considered period. Only sectors pointing toward the planet at an angle from limb of $\varphi < -10°$ are considered. Sectors 0–3 are excluded from the analysis.
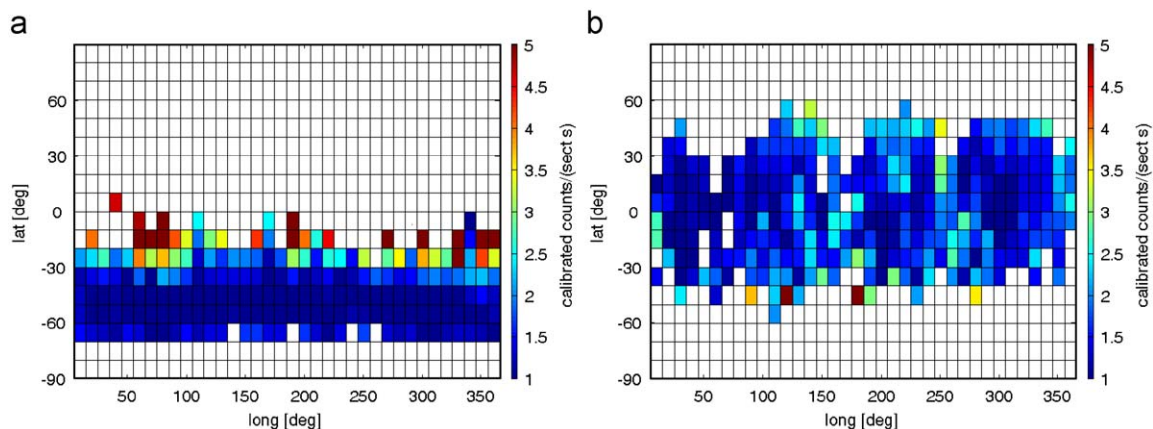
Fig. 10. NPI signal (counts/(s sector)) mapped on Mars surface in planetographic coordinates, for 2004 (a) and 2005 (b) when MEX position is in the deep shadow. Sectors 0–3 are excluded from the analysis.

we cannot be completely sure that the UV contamination is fully removed in our analysis.

- No systematic IMF clock angle dependence is evident from this statistical study. This suggests that there are no pick-up atmospheric ions generating ENAs as expected or, if they are present, the ENA flux is smaller than $6 \times 10^6 \, (\text{cm}^2 \, \text{sr} \, \text{s})^{-1}$ in the analysed energy range.
- A signal less than the intrinsic error $3 \times 10^6 \, (\text{cm}^2 \, \text{sr} \, \text{s})^{-1}$ coming from the anti-Mars direction in 2005, when MEX is in the North-Dusk side, seems related more to bad sector inter-calibration or bright stars in the instrument FOV than to neutral atoms.

We have investigated the existence of ENAs related to specific planet locations with the following results:

- Planetographic-coordinate maps show no relation with the magnetic anomalies, thus excluding the presence of strong ENA signal from close-to-planet magnetic loops.
- Other possible ENA signals are lower than the intrinsic error (flux upper limit is $3 \times 10^6 \, (\text{cm}^2 \, \text{sr} \, \text{s})^{-1}$).

Further analysis is needed in order to completely exclude instrumental and/or UV effects. Our analysis shows that particular attention should be devoted to the preparation of data when performing statistical studies with the NPI data. Alternatively, case study analyses of each sector response versus time can be performed to record intense ENA signals.

Acknowledgments

References

Barabash, S., Holmstrom, M., Lukyanov, A., Kallio, E., 2002. Energetic neutral atoms at Mars, 4. Imaging of planetary oxygen. J. Geophys. Res. 107 (A10), 1280.

Barabash, S., Lundin, R., Andersson, H., Gimholt, J., Holmstrom, M., Norberg, O., Yamauchi, M., Asamura, K., Coates, A.J., Linder, D.R., Kataria, D.O., Curtis, C.C., Hsieh, K.C., Sandel, B.R., Fedorov, A., Grigoriev, A., Budnik, E., Grande, M., Carter, M., Reading, D.H., Koskinen, H., Kallio, E., Riihela, P., Säles, T., Kozyra, J., Krupp, N., Livi, S., Woch, J., Luhmann, J., McKenna-Lawlor, S., Orsini, S., Cerulli-Irelli, R., Maggi, M., Morbidini, A., Mura, A., Milillo, A., Roelof, E., Williams, D., Sauvaud, J.-A., Thocaven, J.-J., Moreau, T., Winningham, D., Frahm, R., Scherrer, J., Sharber, J., Wurz, P., Bochsler, P., 2004. ASPERA-3: analyser of space plasmas and energetic ions for Mars Express. In: Wilson, A. (Ed.), Mars Expresss: The Scientific Payload, Vol. SP-1240. ESA Special Publication, pp. 121–139.

Brain, D.A., Mitchell, D.L., Halekas, J.S., 2006. The magnetic field draping direction at Mars from April 1999 through August 2004. Icarus 182 (2).

Brinkfeldt, K., 2005. Instrumentation for energetic neutral atom measurements at Mars, Venus, and the Earth, IRF Scientific Report 288, ISSN 0284-1703, ISBN 91-7305-993-5, November.

Brinkfeldt, K., et al., 2006. First ENA observations at Mars: solar-wind ENAs on the nightside. Icarus 182 (2), 439–447.

Fedorov, A., Budnik, E., The ASPERA-3 team, 2006. Structure of the Martian wake. Icarus 182 (2), 329.

Futaana, Y., Barabash, S., Grigoriev, A., Holmström, M., Kallio, E., son Brandt, P.C., Gunell, H., Brinkfeldt, K., Lundin, R., Andersson, H., et al., 2006. First ENA observations at Mars: subsolar ENA jet. Icarus 182 (2), 413–423.

Galli, A., Wurz, P., Barabash, S., Grigoriev, A., Gunell, H., Lundin, R., Holmström, M., Fedorov, A., 2006. Energetic hydrogen and oxygen atoms observed on the nightside of Mars. Space Sci. Rev. 126, 267–297.

Galli, A., Wurz, P., Kallio, E., Ekenback, A., Holmström, M., Barabash, S., Grigoriev, A., Futaana, Y., Fok, M.-C., Gunell, H., 2008. The tailward flow of energetic neutral atoms observed at Mars. J. Geophys. Res., in press.

Gunell, H., Brinkfeldt, K., Holmström, M., son Brandt, P.C., Barabash, S., Kallio, E., Ekenbäck, A., Futaana, Y., Lundin, R., Andersson, H., 2006. First ENA observations at Mars: charge exchange ENAs produced in the magnetosheath. Icarus 182 (2), 431–438.

Holmström, M., Barabash, S., Kallio, E., 2002. Energetic neutral atoms at Mars: I. imaging of solar wind protons. J. Geophys. Res. 107 (A10), 1277.

Holmstrom, M., Brinkfeldt, K., Barabash, S., Lundin, R., 2006. Observations in the Shadow of Mars by the Neutral Particle Imager. In: Ip, W.-H., Bhardwaj, A. (Eds.), Advances in Geosciences, vol. 3, pp. 37–50.

Johnson, R.E., Luhmann, J.G., 1998. Sputter contribution to the atmospheric corona on Mars. J. Geophys. Res. 103 (E2), 3649–3653.

Kallio, E., 1996. An empirical model of the solar wind flow around Mars. J. Geophys. Res. 101, 11133–11147.

Kallio, E., Barabash, S., 2001. Atmospheric effects of precipitating energetic hydrogen atoms on the martian atmosphere. J. Geophys. Res. 106 (A1), 165–177.

Kallio, E., Luhmann, J.G., Barabash, S., 1997. Charge exchange near Mars: the solar wind absorption and energetic neutral atom production. J. Geophys. Res. 102 (22), 22183–22197.

Kallio, E., Barabash, S., Brinkfeldt, K., Gunell, H., Holmström, M., Futaana, Y., Schmidt, W., et al., 2006. Energetic neutral atoms (ENA) at Mars: properties of the hydrogen atoms produced upstream of the Martian bow shock and implications for ENA sounding technique around non-magnetized planets. Icarus 182 (2), 448–463.

Lichtenegger, H., Lammer, H., Stumptner, W., 2002. Energetic neutral atoms at Mars: 3. Flux and energy distributions of planetary energetic H atoms. J. Geophys. Res. 107 (A10), 1279.

Milillo, A., Mura, A., Orsini, S., Massetti, S., D'Amicis, R., Frahm, R.A., Kallio, E., son Brandt, P.C., Sotirelis, T., Barabash, S., The ASPERA-3 Team, 2007. MEX/ASPERA-3 NPI data statistical analysis, Internal Note, INAF/IFSI-2007-08.

Mitchell, D.L., Lillis, R.J., Lin, R.P., Connerney, J.E.P., Acuna, M.H., 2007. A global map of Mars' crustal magnetic field based on electron reflectometry. J. Geophys. Res. 112, E01002.

Mura, A., Milillo, A., Orsini, S., Kallio, E., Barabash, S., 2002. Energetic neutral atom at Mars II: imaging of the solar wind-Phobos interaction. J. Geophys. Res. 107, doi:10.1029/2001JA000328.

Mura, A., Orsini, S., Milillo, A., Kallio, E., Galli, A., Barabash, S., The ASPERA-3 team, 2007. ENA detection in the dayside of Mars: ASPERA-3 NPD statistical study. Planetary and Space Science.

Purucker, M., Ravat, D., Frey, H., Voorhies, C., Sabaka, T., Acuna, M., 2000. An altitude-normalized magnetic map of mars and its interpretation. Geophys. Res. Lett. 27, 2449–2452.